Comparative study of evaluation of primary isoclinic data by various spatial domain methods in digital photoelasticity

M Ramji[1], **V Y Gadre**[2], and **K Ramesh**[1]*
[1]Department of Applied Mechanics, Indian Institute of Technology, Madras, Chennai, India
[2]Department of Mechanical Engineering, Indian Institute of Technology, Kanpur, India

The manuscript was received on 21 March 2005 and was accepted after revision for publication on 13 March 2006.

DOI: 10.1243/03093247JSA127

Abstract: With the advent of PC-based digital image processing systems, automation of parameter estimation based on intensity processing from the entire field has now become simpler. Various methods for obtaining the isoclinic parameter using plane, circular, and mixed polariscopes have been reported in the literature. A comparative study has been conducted on the performance of these methods both qualitatively and quantitatively. The focus of the study is on how these algorithms provide the basic isoclinic data. To illustrate the performance, theoretically simulated and experimentally recorded images for a ring under diametral compression is used. The role of background light intensity and quarter-wave plate mismatch on the experimental evaluation of isoclinic data is brought out.

Keywords: digital photoelasticity, phase shifting, polarization stepping, isoclinics, isochromatic–isoclinic interaction, quarter-wave plate error

1 INTRODUCTION

Photoelasticity is an optical method of experimental stress analysis, which yields a whole field representation of principal stress difference and its orientation in the form of fringes. With cost effective digital image processing systems it has now become possible to obtain the fringe order and isoclinic data at every pixel in the domain [**1**]. Data acquisition in digital photoelasticity incorporates various techniques that are primarily based on processing the intensity information recorded by digital means. These techniques can be broadly classified as

1 Phase-shifting technique (PST) [**2–12**]
2. Fourier transform approach [**13**, **14**]
3. Polarization stepping [**15–19**]
4. Load stepping [**20–22**]

The most widely used digital photoelastic technique is the six-step PST in which a circularly polarized light is incident on the model [**2**, **4**]. These methods have been used primarily to evaluate the isochromatic fringe order. The initial developments in digital photoelasticity were confined to the evaluation of isochromatic data. This is because a variety of problems such as the evaluation of the stress concentration factor, the stress intensity factor and contact stress parameters require only isochromatic data. Further comparison between different designs can be done just based on the visual appreciation of the isochromatic data. Photoelasticity by itself gives only the difference in principal stresses or normal stresses. If individual stress components are required then stress separation techniques need to be adopted. To employ stress separation techniques apart from isochromatic data isoclinic values are also required. Further, many algorithms that calculate isochromatic data in digital photoelasticity indirectly use isoclinic data. Thus, any effort in evaluating isoclinics accurately is not only useful for employing stress separation techniques but can also help to improve the accuracy of evaluation of even isochromatic data.

The phase-shifting methods reported by Kihara [**5**, **10**], Dupré *et al.* [**6**], Sarma *et al.* [**7**], Mangal and Ramesh [**9**], Nurse [**11**], and Lei Zhenkun *et al.* [**12**]

* *Corresponding author: Department of Applied Mechanics, Indian Institute of Technology, Madras, Chennai 600 036, India. email: kramesh@iitm.ac.in*

use a plane polarized light incident on the model for data acquisition. Of these methods, Kihara and Dupré *et al.* have also included a quarter-wave plate apart from an analyser to analyse the exit light from the model. Among all these phase-shifting methods only Lei Zhenkun *et al.* have used a white light for model illumination while others have used a monochromatic light source.

The methodology of Morimoto *et al.* [**13**] and Lesniak and Zickel [**14**] lies in the frequency domain. The Fourier transform technique of Morimoto *et al.* [**13**] requires a large number of images to be processed and it is yet to acquire wider acceptance among digital photoelasticians. In polarization stepping, the polarizer and analyser are either kept crossed [**15–17**] or parallel [**18**]. In order to minimize the isochromatic interaction on isoclinic evaluation, the use of multiple loads [**9**] or multiple wavelengths [**10–12**, **19**] are suggested. Although load-stepping [**20–22**] methods are generally developed for fractional retardation determination, Mangal and Ramesh [**9**] proposed the use of multiple loads to minimize the interaction of isochromatics on the evaluation of isoclinics.

Evaluation of the isoclinic parameter is comparatively easy while determining it manually, but automated evaluation has several problems. A comparative study of the algorithms mentioned would help in identifying those algorithms that have a minimal problem in the evaluation of isoclinics due to numerical inaccuracies and interaction of isochromatics in isoclinic evaluation. With this in view, for a few selected spatial domain methods, theoretically simulated phase-shifted images are generated to check the numerical behaviour of these techniques. For each of these methods, the isoclinics are also obtained from experimentally recorded images. The study is done under similar conditions to obtain a comparative statement. This comparison is done for the evaluation of the isoclinic parameter only. The focus is on how these algorithms provide the basic isoclinic data. Though the basic isoclinic data can be improved by appropriate post-processing, the use of post-processing methods [**19**, **23**, **24**] in isoclinic evaluation is not considered in the present study. The role of background intensity and quarter-wave plate mismatch on processing the experimentally recorded intensity patterns is highlighted. For completeness, the various optical arrangements used and the method of isoclinic calculation from the intensity information by various methods are briefly summarized.

The use of phase-shifting techniques for designing digital polariscopes has come to stay and many commercial polariscopes have adopted this technique [**25–28**]. Thus identification of algorithms that provide more accurate primary isoclinic data would be of interest to commercial polariscope designers.

2 INTENSITY EQUATION FOR THE GENERIC ARRANGEMENT OF OPTICAL ELEMENTS IN A POLARISCOPE

The generic optical arrangement for intensity recording in digital photoelasticity is shown in Fig. 1. In PST methods based on circular polariscopes, the first quarter-wave plate is kept at either $\xi = 135^\circ$ or 45°. Using Jones' calculus (for $\xi = 135^\circ$) the intensity of light transmitted is [**1**]

$$I_i = \frac{I_a}{2} + \frac{I_a}{2}[\sin 2(\beta - \eta)\cos\delta - \sin 2(\theta - \eta)\cos 2(\beta - \eta)\sin\delta] \qquad (1)$$

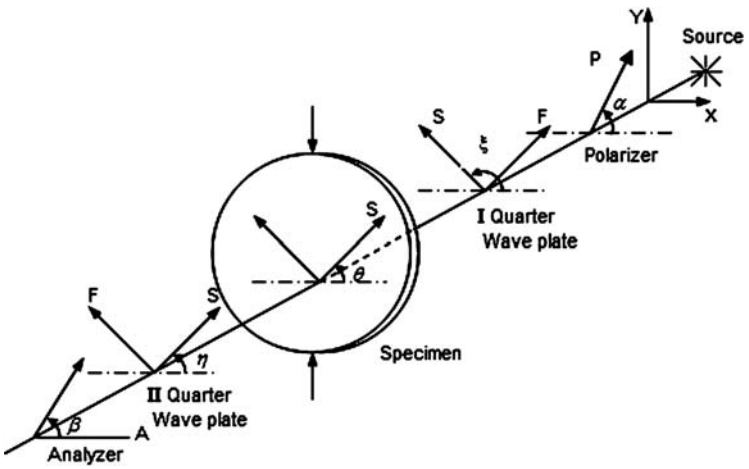

Fig. 1 Generic arrangement of a circular polariscope to employ phase-shifting methodology

Similarly, for a generic plane polariscope with the polarizer at an angle α and analyser at an angle β, the intensity of light transmitted is [**1**]

$$I_i = I_a\left[\cos^2\frac{\delta}{2}\cos^2(\beta-\alpha)+\sin^2\frac{\delta}{2}\cos^2(\beta+\alpha-2\theta)\right] \tag{2}$$

In many algorithms, the influence of background light is modelled as an additional term I_b in the intensity equation.

3 OPTICAL ARRANGEMENTS FOR CIRCULAR, PLANE, AND MIXED POLARISCOPES

3.1 Optical arrangements of algorithms using the circular polariscope

The most commonly used algorithms for isoclinic evaluation based on the circular polariscope are the six-step phase-shifting algorithms proposed by Patterson and Wang [**2**] and Ajovalasit *et al.* [**4**]. The algorithm by Ajovalasit *et al.* uses both left and right circularly polarized light. The optical arrangements for the above-mentioned six-step phase-shifting algorithms are given in Table 1. In addition to the optical arrangements, the table also has the equation for isoclinic parameter evaluation.

3.2 Optical arrangements of algorithms using the plane polariscope

Many algorithms have been proposed for the evaluation of isoclinics using a plane polariscope [**7–13**, **15–19**]. Algorithms based on phase-shifting polarization stepping using a monochromatic as well as a white light source are reported. The optical arrangements for some of the commonly used algorithms are given in Table 2. In addition to the optical arrangements, an equation for isoclinic parameter evaluation and the arc tangent function used is mentioned.

Table 1 Polariscope arrangements, intensity equations, isoclinic evaluation, and arc tangent function used for circular polariscope based methods

ξ	η	β	Intensity equation	Isoclinic evaluation	Arc tangent function used
Patterson and Wang					
$3\pi/4$	0	$\pi/4$	$I_1 = I_b + \frac{I_a}{2}(1+\cos\delta)$	$\theta_c = \frac{1}{2}\tan^{-1}\left(\frac{I_5-I_3}{I_4-I_6}\right)$	atan()
$3\pi/4$	0	$3\pi/4$	$I_2 = I_b + \frac{I_a}{2}(1-\cos\delta)$	$= \frac{1}{2}\tan^{-1}\left(\frac{I_a\sin\delta\sin 2\theta}{I_a\sin\delta\cos 2\theta}\right)$	
$3\pi/4$	0	0	$I_3 = I_b + \frac{I_a}{2}(1-\sin 2\theta\sin\delta)$	for $\sin\delta \neq 0$	
$3\pi/4$	$\pi/4$	$\pi/4$	$I_4 = I_b + \frac{I_a}{2}(1+\cos 2\theta\sin\delta)$		
$3\pi/4$	$\pi/2$	$\pi/2$	$I_5 = I_b + \frac{I_a}{2}(1+\sin 2\theta\sin\delta)$		
$3\pi/4$	$3\pi/4$	$3\pi/4$	$I_6 = I_b + \frac{I_a}{2}(1-\cos 2\theta\sin\delta)$		
Ajovalasit *et al.*					
$3\pi/4$	$\pi/4$	$\pi/2$	$I_1 = I_b + \frac{I_a}{2}(1+\cos\delta)$	$\theta_c = \frac{1}{2}\tan^{-1}\left(\frac{I_5-I_3}{I_4-I_6}\right)$	atan()
$3\pi/4$	$\pi/4$	0	$I_2 = I_b + \frac{I_a}{2}(1-\cos\delta)$	$= \frac{1}{2}\tan^{-1}\left(\frac{I_a\sin\delta\sin 2\theta}{I_a\sin\delta\cos 2\theta}\right)$	
$3\pi/4$	0	0	$I_3 = I_b + \frac{I_a}{2}(1-\sin 2\theta\sin\delta)$	for $\sin\delta \neq 0$	
$3\pi/4$	$\pi/4$	$\pi/4$	$I_4 = I_b + \frac{I_a}{2}(1+\cos 2\theta\sin\delta)$		
$\pi/4$	0	0	$I_5 = I_b + \frac{I_a}{2}(1+\sin 2\theta\sin\delta)$		
$\pi/4$	$3\pi/4$	$\pi/4$	$I_6 = I_b + \frac{I_a}{2}(1-\cos 2\theta\sin\delta)$		

Table 2 Polariscope arrangements, intensity equations, isoclinic evaluation, and arc tangent function used for plane polariscope based methods

α	β	Intensity equation	Isoclinic evaluation	Arc tangent function used
Sarma *et al.*				
$\pi/2$	$\pi/2$	$I_1 = I_a\left(\cos^2\frac{\delta}{2} + \sin^2\frac{\delta}{2}\cos^2 2\theta\right)$	$\theta_c = \frac{1}{2}\tan^{-1}\left(\frac{2I_2}{I_1 + I_2 - 2I_3}\right)$	atan()
$\pi/2$	0	$I_2 = I_a\left(\sin^2\frac{\delta}{2}\sin^2 2\theta\right)$	$= \frac{1}{2}\tan^{-1}\left(\frac{I_a \sin^2 \delta/2 \sin 2\theta}{I_a \sin^2 \delta/2 \cos 2\theta}\right)$	
$\pi/2$	$\pi/4$	$I_3 = \frac{I_a}{2}\left(1 - \sin^2\frac{\delta}{2}\sin 4\theta\right)$	for $\sin^2\frac{\delta}{2} \neq 0$	
Mangal and Ramesh				
0	$\pi/2$	$I_1 = I_b + I_a \sin^2\frac{\delta}{2}\sin^2 2\theta$	$\theta_c = \frac{1}{4}\tan^{-1}\left(\frac{I_3 - I_2}{I_4 - I_1}\right)$	atan2()
$\pi/4$	$\pi/2$	$I_2 = I_b + \frac{I_a}{2}\left(1 - \sin^2\frac{\delta}{2}\sin 4\theta\right)$	$= \frac{1}{4}\tan^{-1}\left(\frac{I_a \sin^2 \delta/2 \sin 4\theta}{I_a \sin^2 \delta/2 \cos 4\theta}\right)$	
0	$\pi/4$	$I_3 = I_b + \frac{I_a}{2}\left(1 + \sin^2\frac{\delta}{2}\sin 4\theta\right)$	for $\sin^2\frac{\delta}{2} \neq 0$	
$\pi/4$	$3\pi/4$	$I_4 = I_b + I_a \sin^2\frac{\delta}{2}\cos^2 2\theta$		
$\pi/4$	$\pi/4$	$I_5 = I_b + I_a\left(\cos^2\frac{\delta}{2} + \sin^2 \delta/\sin^2 2\theta\right)$		
0	0	$I_6 = I_b + I_a\left(\cos^2\frac{\delta}{2} + \sin^2\frac{\delta}{2}\cos^2 2\theta\right)$		
Brown and Sullivan/Petrucci (light source is changed to white light for θ_c calculation – refer to text)				
$\pi/2$	0	$I_1 = I_b + I_a \sin^2\frac{\delta}{2}\sin^2 2\theta$	$\theta_c = \frac{1}{4}\tan^{-1}\left(\frac{I_4 - I_2}{I_3 - I_1}\right)$	atan2()
$5\pi/8$	$\pi/8$	$I_2 = I_b + \frac{I_a}{2}\sin^2\frac{\delta}{2}(1 - \sin 4\theta)$	$= \frac{1}{4}\tan^{-1}\left(\frac{I_a \sin^2 \delta/2 \sin 4\theta}{I_a \sin^2 \delta/2 \cos 4\theta}\right)$	
$3\pi/4$	$\pi/4$	$I_3 = I_b + I_a \sin^2\frac{\delta}{2}\cos^2 2\theta$	for $\sin^2\frac{\delta}{2} \neq 0$	
$7\pi/8$	$3\pi/8$	$I_4 = I_b + \frac{I_a}{2}\sin^2\frac{\delta}{2}(1 + \sin 4\theta)$		
Chen and Lin				
0	0	$I_1 = I_a\left(1 - \sin^2 2\theta \sin^2\frac{\delta}{2}\right)$	$\theta_c = \frac{1}{4}\tan^{-1}\left(\frac{I_1'' + I_3'' - 2I_2''}{I_3'' - I_1''}\right)$	atan2()
$\pi/8$	$\pi/8$	$I_2 = I_a\left[1 - \frac{1}{2}(\sin 2\theta - \cos 2\theta)^2 \sin^2\frac{\delta}{2}\right]$	$= \frac{1}{4}\tan^{-1}\left(\frac{I_a \sin^2 \delta/2 \sin 4\theta}{I_a \cos^2 \delta/2 \cos 4\theta}\right)$	
$\pi/4$	$\pi/4$	$I_3 = I_a\left(1 - \cos^2 2\theta \sin^2\frac{\delta}{2}\right)$	for $\sin^2\frac{\delta}{2} \neq 0$	
Lei Zhenkun *et al.*				
$\pi/2$	0	$I_1 = I_b + I_a \sin^2\frac{\delta}{2}\sin^2 2\theta$	$\theta_c = \frac{1}{4}\tan^{-1}\left(\frac{I_4 - I_2}{I_5 - I_1}\right)$	atan2()
$\pi/2$	$\pi/4$	$I_2 = I_b + \frac{I_a}{2}\left(1 - \sin^2\frac{\delta}{2}\sin 4\theta\right)$	$= \frac{1}{4}\tan^{-1}\left(\frac{I_a \sin^2 \delta/2 \sin 4\theta}{I_a \sin^2 \delta/2 \cos 4\theta}\right)$	
0	$\pi/4$	$I_4 = I_b + \frac{I_a}{2}\left(1 + \sin^2\frac{\delta}{2}\sin 4\theta\right)$	for $\sin^2\frac{\delta}{2} \neq 0$	
$\pi/4$	$3\pi/4$	$I_5 = I_b + I_a \sin^2\frac{\delta}{2}\cos^2 2\theta$		

In phase shifting, the polarizer and analyser are kept at arbitrary positions to record intensity data. If all the possible combinations of orientations of the polarizer and analyser are taken in steps of $\pi/4$, then only six intensity equations turn out to be unique [**8**]. These six images are used by Mangal and Ramesh [**9**] to evaluate the isoclinics. The phase-shifting algorithm proposed by Sarma *et al.* [**7**] is

more of academic interest and uses the least number of optical arrangements, namely only three, to evaluate both isochromatics and isoclinics.

In polarization stepping the polarizer and analyser are either kept crossed or parallel. Intensity is recorded for different orientations of the polarizer. Brown and Sullivan [**15**] used a polarization stepping approach in which four images are recorded with a crossed polarizer and analyser in steps of $\pi/8$ radians. Chen and Lin [**18**] proposed a methodology in which three bright-field images in a plane polariscope arrangement are obtained. From these bright-field images, dark-field images are constructed using the trigonometric identity and the concept of image division as

$$I_i'' = 1 - \frac{I_i}{I_{ui}} \tag{3}$$

where I_i'' is the dark-field image intensity and I_{ui} is the intensity corresponding to the unloaded image. The new modified intensity is used for isoclinic estimation (Table 2). The construction of normalized dark-field images from the bright-field images is an important step in this method.

In order to minimize the role of isochromatic interaction on isoclinics the use of white light for intensity recording has also been proposed [**12**, **19**]. Of these, the methodology proposed by Petrucci [**19**] is a polarization stepping method similar to that of Brown and Sullivan [**15**] except that the model is illuminated by a white light source. Petrucci [**19**] observed that instead of using intensity from any one of the image planes, the accuracy of evaluation is improved if summations of these intensities are used. Thus, the isoclinic is determined by

$$\theta_c = \frac{1}{4}\tan^{-1}\left(\frac{I_4 - I_2}{I_3 - I_1}\right) = \frac{1}{4}\tan^{-1}\left[\frac{(I_{4,R} + I_{4,G} + I_{4,B}) - (I_{2,R} + I_{2,G} + I_{2,B})}{(I_{3,R} + I_{3,G} + I_{3,B}) - (I_{1,R} + I_{1,G} + I_{1,B})}\right] \tag{4}$$

where $I_{i,j}$ ($i = 1, 2, 3, 4$; $j = $ R, G, B) correspond to pixel grey levels of R, G, and B planes for the analyser positions of 0, 22.5, 45, and 67.5° respectively. Lei Zhenkun *et al.* [**12**] combined colour imaging with phase shifting for the whole field determination of the isoclinic parameter. They used five images for the isoclinic evaluation and named their technique the five-step colour phase-shifting technique (FCPST). The isoclinic is determined by

$$\theta = \frac{1}{4}\tan^{-1}\left(\frac{I_4 - I_2}{I_5 - I_1}\right) = \frac{1}{4}\tan^{-1}\left(\frac{(I_{4,R} - I_{2,R}) + (I_{4,G} - I_{2,G}) + (I_{4,B} - I_{2,B})}{(I_{5,R} - I_{1,R}) + (I_{5,G} - I_{1,G}) + (I_{5,B} - I_{1,B})}\right) \tag{5}$$

3.3 Optical arrangements of algorithms using the mixed polariscope

The mixed polariscope is one in which the incident light on the model is plane polarized but the exit light is analysed by a combination of a quarter-wave plate and analyser. Kihara [**5**] has proposed a method with eight optical arrangements and Dupré *et al.* [**6**] have proposed a method with four optical arrangements. In both of these methods, the background light intensity is not explicitly accounted for. The optical arrangements and the equations for isoclinic determination for these algorithms are mentioned in Table 3.

4 COMPARATIVE STUDY OF VARIOUS METHODS

4.1 Performance of the algorithms on theoretically simulated images

For each of the algorithms mentioned in the previous sections that use monochromatic light for illumination, for the problem of a ring under diametral compression (inner diameter = 40 mm, outer diameter = 80 mm, thickness = 5.05 mm, load = 503 N, $F_\sigma = 11.23$) phase-shifted images are theoretically simulated as in Tables 1, 2, and 3. From these images the value of the isoclinic is calculated using the respective arc tangent functions mentioned in Tables 1 to 3 and the isoclinics are plotted in steps of 10° over the model domain (Fig. 2). The figure also gives the isoclinics in steps of 10° obtained by analytical solution [**29**, **30**]. For brevity, the isoclinic plots for all the methods are not reported as the results obtained are similar because they are free of experimental inaccuracies. The results are grouped into two categories and a representative plot for methods that employ a quarter-wave plate(s) and a representative plot for plane polariscope methods is given. The figure also gives the isoclinics in steps of 10° obtained by analytical solution [**30**]. It can be seen from the images that for all the methods the geometric shape of the isoclinic contours matches with theory only with small perturbations. For methods based on the plane polariscope (Fig. 2b), the skeletons

Table 3 Polariscope arrangements, intensity equations, isoclinic evaluation, and arc tangent function used for mixed polariscope algorithms

α	η	β	Intensity equation	Isoclinic evaluation	Arc tangent function used
Dupré *et al.*					
0	—	0	$I_1 = I_a$ (model not loaded)	$\theta_c = \frac{1}{4}\tan^{-1}\left(\frac{2I_3 - I_1}{I_2 - I_4}\right)$	atan2()
0	—	0	$I_2 = I_a\left(\cos^2\frac{\delta}{2} + \sin^2\frac{\delta}{2}\cos^2 2\theta\right)$	$= \frac{1}{4}\tan^{-1}\left(\frac{I_a \sin^2 \delta/2 \sin 4\theta}{I_a \sin^2 \delta/2 \cos 4\theta}\right)$	
0	—	$\pi/4$	$I_3 = \frac{I_a}{2}\left(1 + \sin^2\frac{\delta}{2}\sin 4\theta\right)$	for $\sin^2\frac{\delta}{2} \neq 0$	
$\pi/4$	—	$\pi/4$	$I_4 = I_a\left(\cos^2\frac{\delta}{2} + \sin^2\frac{\delta}{2}\sin^2 2\theta\right)$		
0	$3\pi/4$	0	$I_5 = \frac{I_a}{2}(1 + \sin 2\theta \sin\delta)$		
Kihara					
0	$\pi/2$	$-\pi/4$	$I_1 = \frac{I_a}{2}(1 + \sin\delta \sin 2\theta)$	$\theta_c = \frac{1}{2}\tan^{-1}\left(\frac{I_1 - I_2}{I_3 - I_4}\right)$	atan()
0	$\pi/2$	$\pi/4$	$I_2 = \frac{I_a}{2}(1 - \sin\delta \sin 2\theta)$	$= \frac{1}{2}\tan^{-1}\left(\frac{I_a \sin\delta \sin 2\theta}{I_a \sin\delta \cos 2\theta}\right)$	
$-\pi/4$	$\pi/2$	$-\pi/4$	$I_3 = \frac{I_a}{2}(1 + \sin\delta \cos 2\theta)$	for $\sin\delta \neq 0$	
$-\pi/4$	$\pi/2$	$\pi/4$	$I_4 = \frac{I_a}{2}(1 - \sin\delta \cos 2\theta)$		
0	$\pi/2$	0	$I_5 = I_a\left(\cos^2\frac{\delta}{2} + \sin^2\frac{\delta}{2}\cos^2 2\theta\right)$		
0	$\pi/2$	$\pi/2$	$I_6 = I_a\left(\sin^2\frac{\delta}{2}\sin^2 2\theta\right)$		
$-\pi/4$	$\pi/4$	$-\pi/4$	$I_7 = I_a\left(\cos^2\frac{\delta}{2} + \sin^2\frac{\delta}{2}\sin^2 2\theta\right)$		
$-\pi/4$	$\pi/4$	$\pi/4$	$I_8 = I_a\left(\sin^2\frac{\delta}{2}\cos^2 2\theta\right)$		

of the isochromatics are seen more predominantly than for either the circular or the mixed polariscope [Fig. 2(a)]. Since mathematically isoclinics are not defined on isochromatic lines, skeletons are observed on an isoclinic plot resembling the isochromatics.

4.2 Performance of the algorithm on experimentally recorded images

In order to study the performance of various algorithms on experimentally recorded phase-shifted images, two sets of experiments were performed, one with a monochrome source and another with a white light source, for the problem of a ring under diametral compression, mentioned earlier. The monochromatic source used is sodium vapour and the intensity of the light transmitted is recorded by a monochrome charge coupled device (CCD) camera (TM-560 PULNiX) having a resolution of 512×512 pixels. Although some researchers have suggested the use of interpolation techniques for improving data obtained from their algorithms [**19**, **23**] these are not implemented here as the focus of this paper is on assessing the quality of the primary data from employing these algorithms.

Figures 3(a) and (b) show the isoclinic plots obtained by the algorithms using a circular polariscope, Figs 3(c) to (g) show the isoclinic plots obtained by various algorithms based on a plane polariscope, and Figs 3(h) and (i) show the isoclinic plots obtained by algorithms using a mixed polariscope. While using white light as a source, the fringes appear in colour. To record images in colour, the Sony 3CCD camera (XC-003P) with a spatial resolution of 752×576 pixels is used. Figures 3(j) and (k) show the isoclinic plots obtained by algorithms based on a plane polariscope using a white light source. In these methods separation of the original composite RGB image into R, G, and B planes is needed for the estimation of the isoclinic parameter. In this work

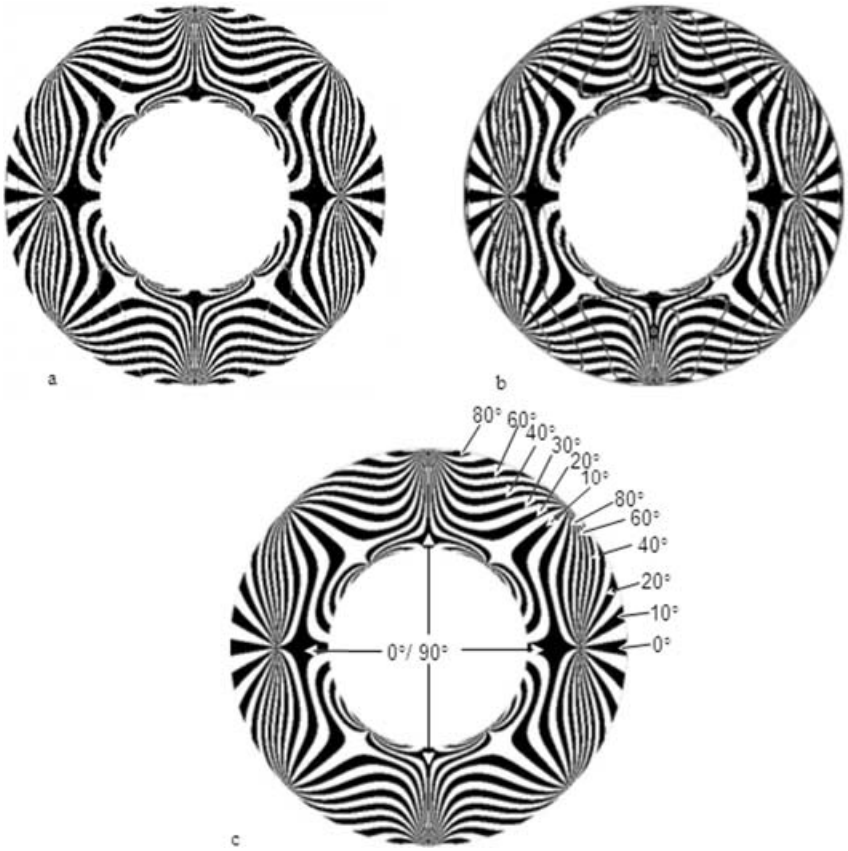

Fig. 2 Isoclinic plots in steps of 10° obtained from theoretically simulated phase-shifted/polarization-stepped images of a ring under diametral compression. (a) Representative plot for circular and mixed polariscope arrangements, (b) representative plot for plane polariscope arrangements, and (c) analytical solution [**29**]

Matrox imaging software is used to obtain R, G, and B planes separately from a composite RGB image.

Figure 3 clearly shows that, in practice, the various methods for isoclinic evaluation, although behaving in a similar manner on theoretically simulated images, have performed in a drastically different fashion on experimentally recorded phase-shifted images. The results of only Figs 3(c), (d), (f), (j), and (k) have various degrees of similarities to those of the theoretical values of isoclinics [**29**] plotted over the whole field [Fig. 2(c)]. In Figs 3(e) and (f) the results correspond to Chen and Lin [**18**] by using two different representations of the dark-field light intensity. Figure 3(e) is obtained using the intensity equation (3) and Fig. 3(f) is obtained by a modified equation (3) as

$$I_i'' = 1 - k\frac{I_i}{I_{ui}} \tag{6}$$

In a theoretical implementation of the Chen and Lin algorithm [Fig. 2(e)], I_a is kept constant at 255 all over the domain, and this is always greater than or equal to the loaded bright-field intensity in the domain. However, experimentally this is not the case, for at some places in the domain the unloaded model intensity becomes less than the loaded model. Hence, in equation (3), the ratio of the loaded intensity to the unloaded one becomes greater than one. To offset this problem a factor k is introduced in equation (6). Typically the value of k for the experimental set-up used lies in the range 0.5–0.7. In this work k is chosen as 0.65.

5 DISCUSSION OF THE RESULTS ON EXPERIMENTALLY RECORDED PHASE-SHIFTED IMAGES

5.1 Qualitative analysis

Figure 3 is a quantitative plot of the isoclinics plotted in steps of 10° for various methods. For a qualitative comparison, it is easy to compare the geometric shape of the plots for each of the algorithms with that of the analytical solution [Fig. 2(c)]. Inspection

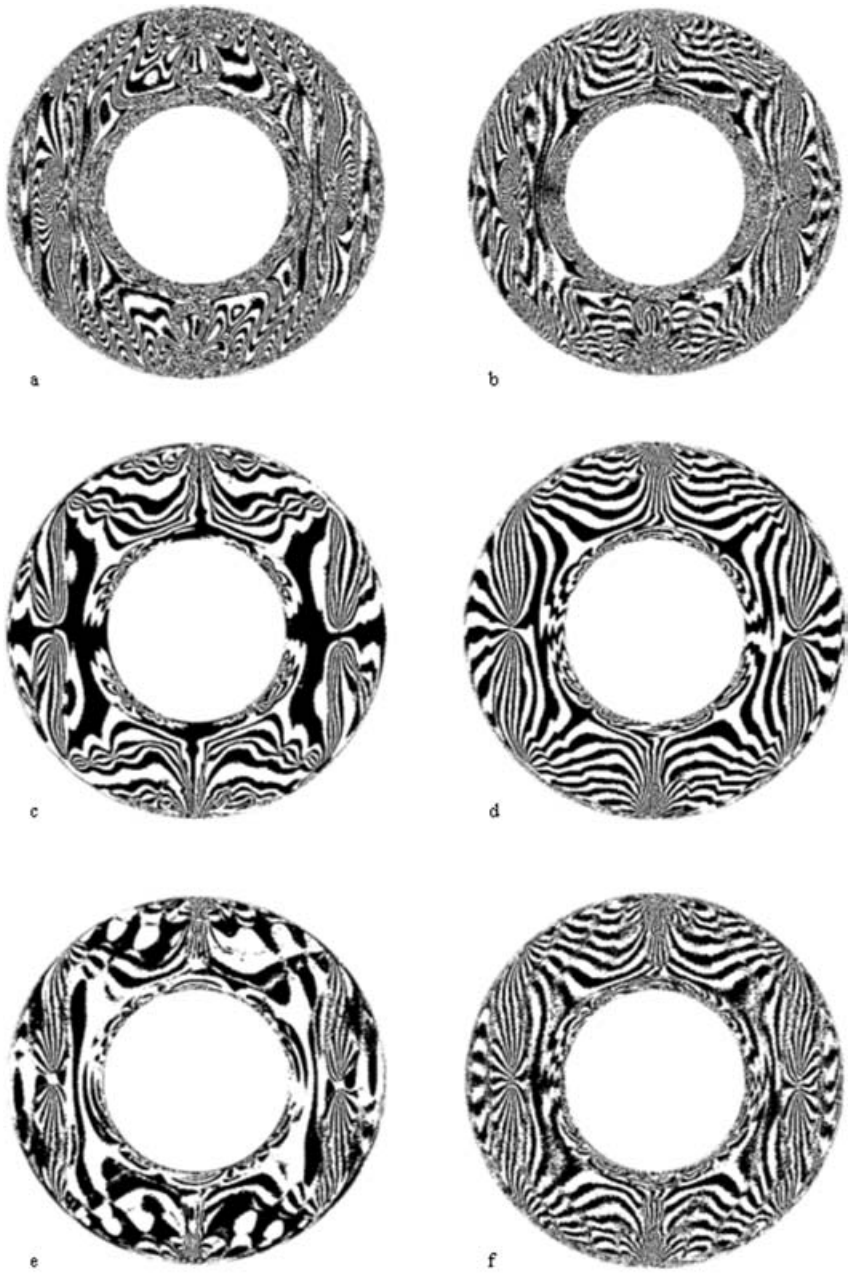

Fig. 3 Isoclinic plots in steps of 10° obtained from the experimentally recorded phase-shifted/polarization-stepped images of a ring under diametral compression by: (a) Patterson and Wang, (b) Ajovalasit *et al.*, (c) Mangal and Ramesh, (d) Brown and Sullivan, (e) Chen and Lin (without adjustment), (f) Chen and Lin (with adjustment), (g) Sarma *et al.*, (h) Dupré *et al.*, (i) Kihara, (j) Petrucci, and (k) Lei Zhenkun *et al.*

of Fig. 3 reveals that in a circular polariscope arrangement, the method of Ajovalasit *et al.* is found to be better compared to that of Patterson and Wang. Among the plane polariscope arrangements the methodologies of Brown and Sullivan and Mangal and Ramesh are found to give an isoclinic pattern close to the theoretically obtained isoclinics. Among the mixed polariscope arrangements, the method of Kihara is found to be better than that of Dupré *et al.* Of methods that use white light as a source, the method of Petrucci is better than that of Lei Zhenkun *et al.*

5.2 Quantitative analysis

The experimentally calculated θ is compared with the θ calculated theoretically for two selected lines of $y/R = 0.25$ and $y/R = 0.5$. Along the line $y/R = 0.5$,

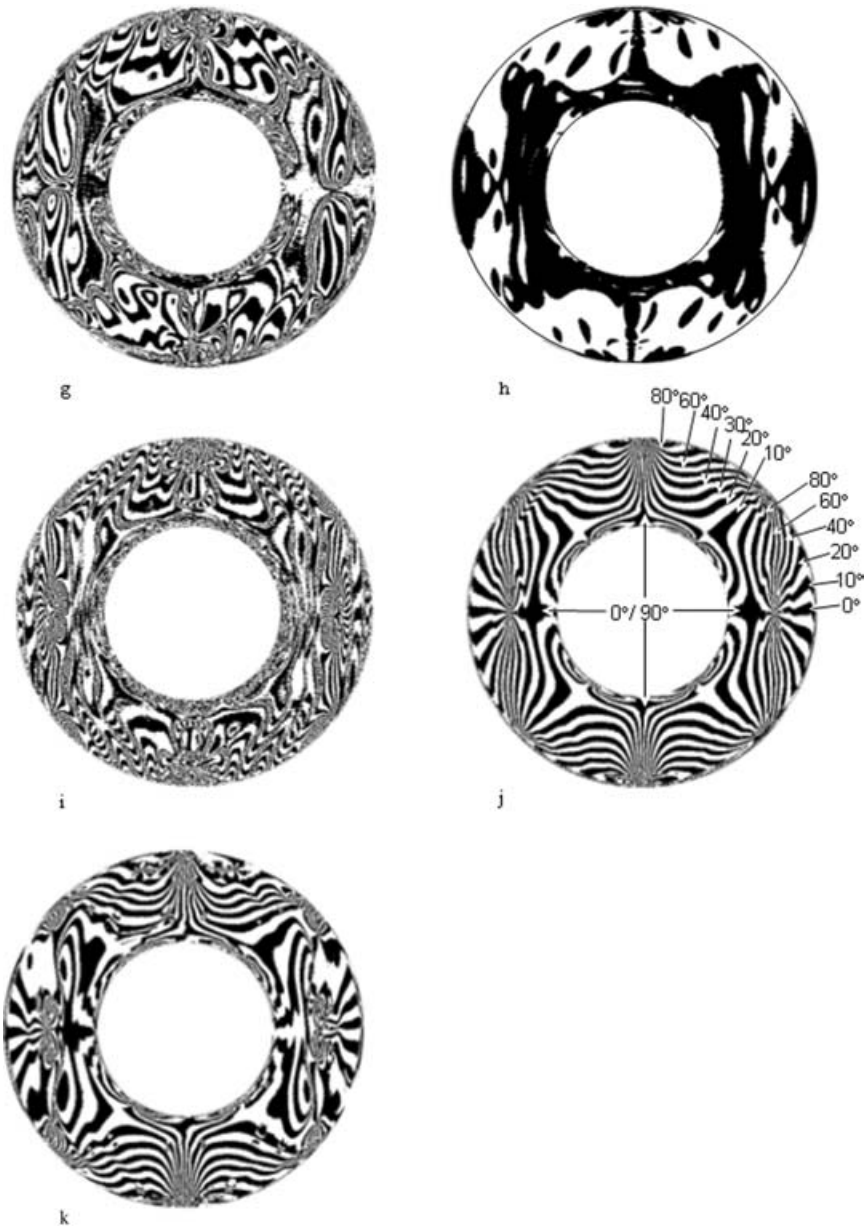

Fig. 3 (Continued)

θ lies in the range $-\pi/4$ to $+\pi/4$ and for the line at $y/R = 0.25$, θ lies in the range $-\pi/2$ to $+\pi/2$. Figure 4 shows the graph obtained for the line $y/R = 0.5$ and Fig. 5 for $y/R = 0.25$ for the methods that use a monochrome light source. In all, eight methods of isoclinic evaluation using a monochrome light source are compared with theory. For clarity, the graphs are drawn for results obtained from three experimental methods at a time compared with theory.

Figure 4(a) shows the graph obtained by the methods of Mangal and Ramesh, Patterson and Wang, and Ajovalasit *et al.* compared with theory. It shows that the results obtained by the methodologies of Patterson and Wang and Ajovalasit *et al.* have sharp spikes and follow the theoretical values only at very small regions. Further, referring to Fig. 4(b), the deviation from theory is far greater for the algorithm of Patterson and Wang than that of Ajovalasit *et al.* This result compares well with those reported by Ajovalasit *et al.* [**4**] for substantiating the use of both left and right circularly polarized lights for data acquisition by the six-step phase-shifting algorithm.

The results obtained by the algorithm of Mangal and Ramesh do not have spikes and the results are much closer to the theory. Figure 4(b) shows the

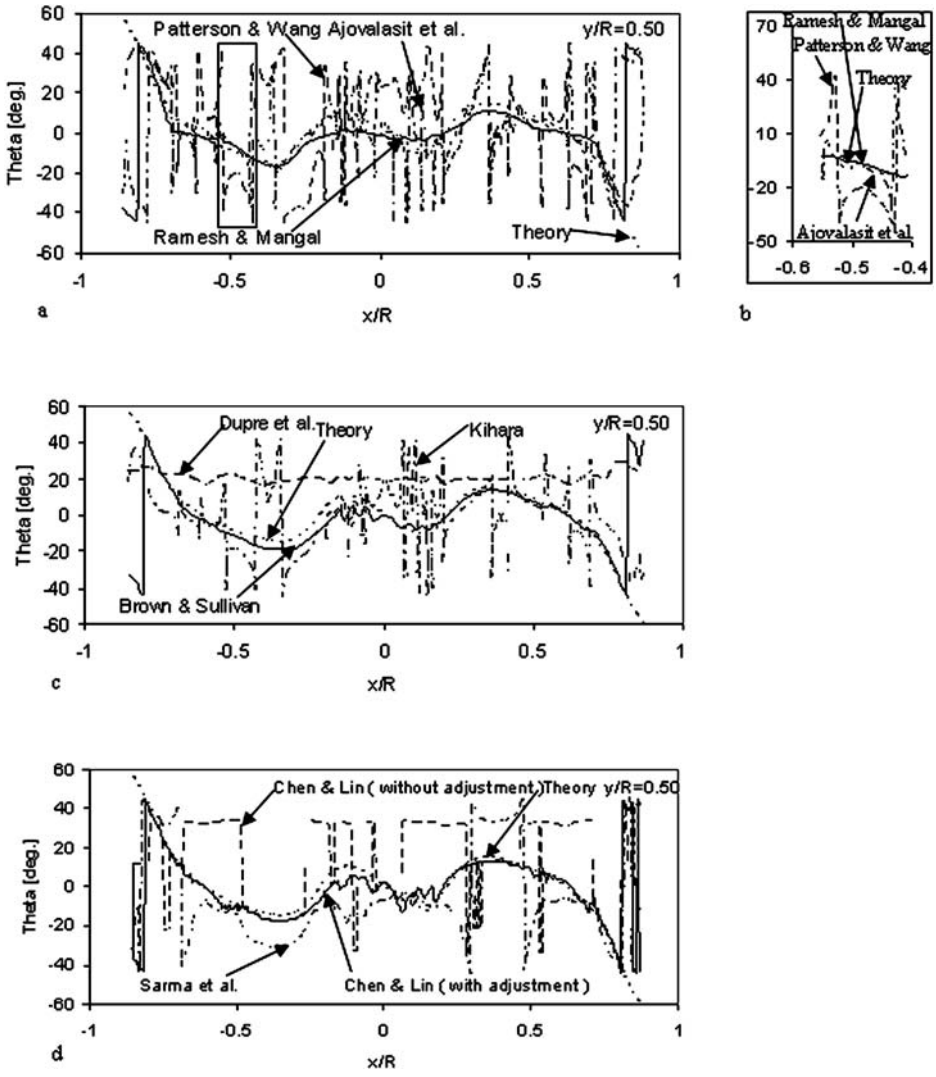

Fig. 4 Comparison of experimental θ with theoretical θ for the line at $y/R = 0.50$: (a) Mangal and Ramesh, Patterson and Wang, Ajovalasit *et al.*, and theory; (b) zoomed portion of the marked rectangular box in Fig. 4(a); (c) Brown and Sullivan, Dupré *et al.*, Kihara, and theory; (d) Chen and Lin, Sarma *et al.*, and theory

graphs obtained from the methods of Brown and Sullivan, Dupré *et al.*, and Kihara compared with theory. It shows that the results obtained by Kihara's technique have sharp spikes and the data follow the trend of the theoretical line in between the spikes. The results obtained by the algorithm of Brown and Sullivan are closer to the theoretical values without any spikes. The algorithm of Dupré *et al.* gives a constant value of the isoclinic over the line, which is absurd. Although theoretically the algorithm of Dupré *et al.* gave good results [Fig. 3(h)], experimentally the method has failed as it has not handled the role of background light intensity properly [**31**]. Following the other algorithms, if the background intensity I_b is added to the equations shown in Table 3, in the absence of the model the expression of the isoclinic by the algorithm of Dupré *et al.* is

$$\theta_c = \frac{1}{4}\tan^{-1}\left(\frac{2I_3 - I_1}{I_2 - I_4}\right) = \frac{1}{4}\tan^{-1}\left(\frac{I_b}{0}\right) \tag{7}$$

In the absence of the model, the isoclinic is not defined and the expression of θ should be found to be indeterminate, which happens in all other

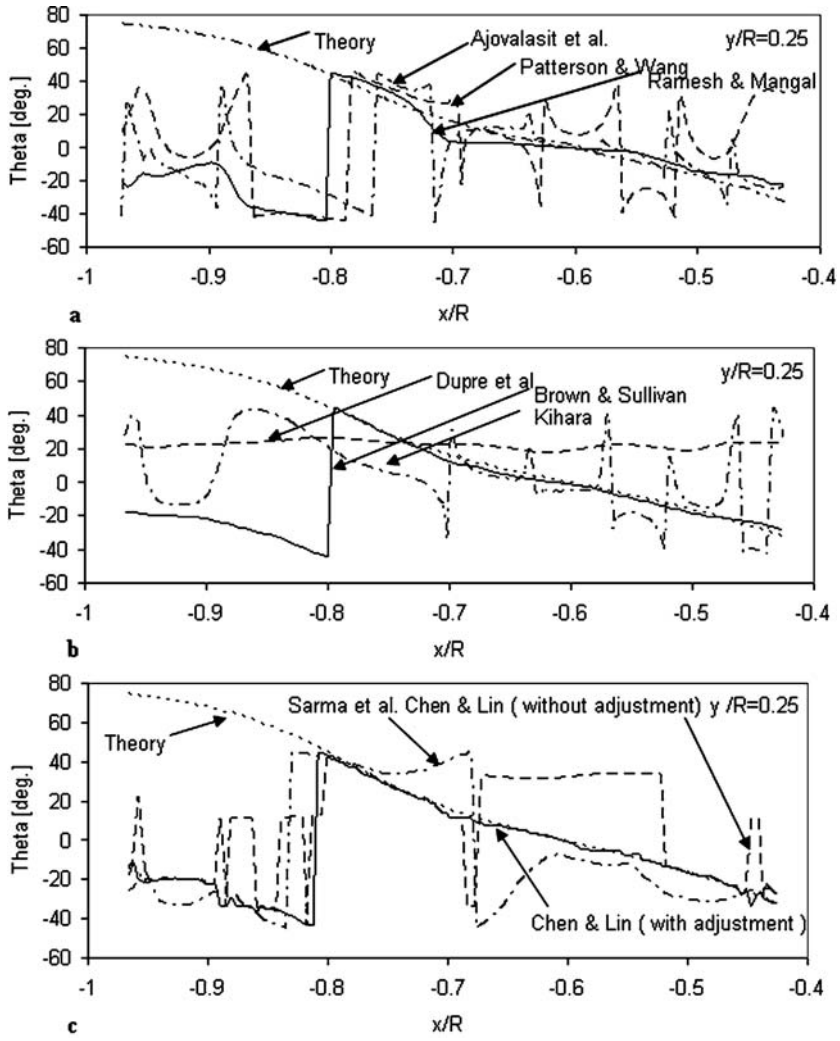

Fig. 5 Comparison of experimental θ with theoretical θ for the line at $y/R = 0.25$: (a) Mangal and Ramesh, Patterson and Wang, Ajovalasit *et al.*, and theory; (b) Brown and Sullivan, Dupré *et al.*, Kihara, and theory; (c) Chen and Lin, Sarma *et al.*, and theory

techniques where the background light intensity is properly accounted for [**31**], but this is not the case in equation (7).

Figure 4(c) shows the graphs obtained from the methods of Chen and Lin [equations (3) and (6)] and Sarma *et al.* and theory for the line at $y/R = 0.5$. It shows that the results obtained by the Sarma *et al.* technique have sharp spikes. The result obtained by the method of Chen and Lin using equation (6) is good and follows the theoretical data, whereas using equation (3) it is quite bad. Algorithms by Sarma *et al.*, Chen and Lin, and Kihara have also not included the background/stray light intensity I_b explicitly in the intensity equations. Although Sarma *et al.* have not taken into account I_b explicitly, they have proposed instead that an image of the unstressed model should be captured in the polariscope when the polarizer and analyser are kept in the crossed position. The intensity values of this image are to be subtracted from all other images before any processing is done. In the methodologies of Chen and Lin and Kihara, if I_b is added as in other methods, the isoclinic parameter is indeterminate when the model is absent [**31**].

The isoclinic values obtained by various methods along the line $y/R = 0.25$ (Fig. 5) are similar in trend to what has been observed for the line $y/R = 0.5$. However, from Fig. 5 it can be seen that none of these algorithms give correct values of θ_c beyond the $-\pi/4$ to $+\pi/4$ range. This is because in most of the methods the arc tangent function returns θ_c in the range of $-\pi/4$ to $+\pi/4$. Thus there is a need to unwrap isoclinic values as well in digital photoelastic analysis.

Figure 6(a) shows the results obtained from the methods of Petrucci, Lei Zhenkun *et al.*, and theory for the line $y/R = 0.5$ and Fig. 6(b) for the line $y/R = 0.25$. For the line $y/R = 0.5$, both of these algorithms give similar results with a minor deviation by Lei Zhenkun *et al.* For the line $y/R = 0.25$ the algorithm of Lei Zhenkun *et al.* has performed poorly in comparison to that of Petrucci. The problem of the isoclinic estimation beyond $\pi/4$ still remains as in other methods.

In summary, the plane polariscope methods in which background light intensity is properly accounted for stand out in the estimation of isoclinics much better than the other methods. There is a need to develop unwrapping algorithms to obtain the isoclinics in the range of $-\pi/2$ to $+\pi/2$.

5.3 Role of the quarter-wave plate mismatch in the isoclinic evaluation

Inspection of Figs 4 and 5 clearly shows that the isoclinic value obtained by any of the methods that use quarter-wave plates (circular and mixed polariscopes) in the optical arrangement is far from theory. The deviation level varies slightly between the methods in the way the optical arrangement is constructed [Fig. 4(b)]. A quarter-wave plate is expected to give a retardation of $\pi/2$ for a specified wavelength. If there is a wavelength mismatch then the retardation can be expressed as

$$\delta = \frac{\pi}{2} + \varepsilon \tag{8}$$

Assuming that the matching wavelength for the quarter-wave plate is λ_{ref}, then for an arbitrary wavelength λ, the error ε caused by the quarter-wave plates is defined as [**32**]

$$\varepsilon = \frac{\pi}{2}\left(\frac{\lambda}{\lambda_{\text{ref}}} - 1\right) \tag{9}$$

In a recent reference [**33**] it has been pointed out that the error ε by a quarter-wave plate is also handedness dependent. In a theoretical simulation, if ε is used for modelling a mismatch of left circularly polarized light then ε' should be used for right circularly polarized light.

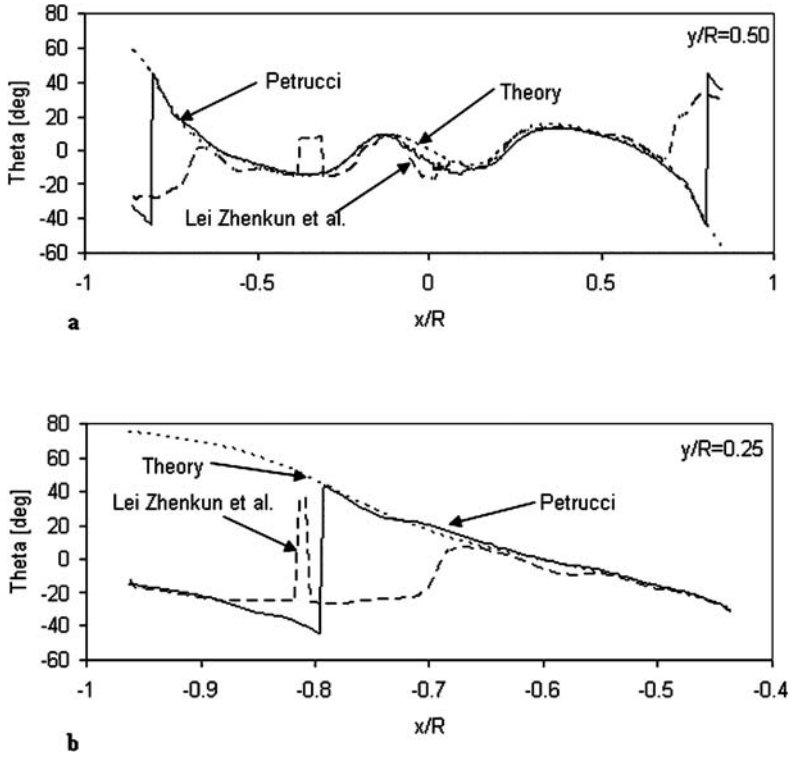

Fig. 6 Comparison of experimental θ with theoretical θ for white light based methods: (a) Petrucci, Lei Zhenkun *et al.*, and theory for the line at $y/R = 0.50$; (b) Petrucci, Lei Zhenkun *et al.*, and theory for the line at $y/R = 0.25$

Table 4 shows the intensity equations incorporating the effect of a quarter-wave plate mismatch for the algorithms of Ajovalasit *et al.*, Patterson and Wang, and Kihara. These are obtained using the symbolic programming language Maple. From the equations of Ajovalasit *et al.* listed in Table 4, if for both left and right circularly polarized light the quarter-wave plate error is assumed to be the same then the isoclinic parameter is

$$\theta_c = \frac{1}{2}\tan^{-1}\left(\frac{I'_5 - I'_3}{I'_4 - I'_6}\right) = \frac{1}{2}\tan^{-1}\left(\frac{I_a \sin\delta \sin 2\theta \cos\varepsilon}{I_a \sin\delta \cos 2\theta \cos\varepsilon}\right) \quad \text{for } \sin\delta \neq 0 \tag{10}$$

Table 4 Polariscope arrangements, intensity equations with quarter-wave plate error by Ajovalasit *et al.*, Patterson and Wang, and Kihara algorithms

I'_i	Intensity equation along with the quarter-wave plate error ε
Ajovalasit *et al.*	
I'_1	$I_b + I_a\left[(1-\cos^2 2\theta \sin^2\varepsilon)\cos^2\frac{\delta}{2} + \cos^2 2\theta \sin^2\varepsilon\right]$
I'_2	$I_b + I_a\left[(1-\cos^2 2\theta \sin^2\varepsilon)\sin^2\frac{\delta}{2}\right]$
I'_3	$I_b + \frac{I_a}{2}[1 + (\cos^2 2\theta + \sin^2 2\theta \cos\delta)\sin\varepsilon - \sin 2\theta \cos\varepsilon \sin\delta]$
I'_4	$I_b + \frac{I_a}{2}[1 + (1-\cos\delta)\sin 2\theta \cos 2\theta \sin\varepsilon + \cos 2\theta \cos\varepsilon \sin\delta]$
I'_5	$I_b + \frac{I_a}{2}[1 + (\cos^2 2\theta + \sin^2 2\theta \cos\delta)\sin\varepsilon + \sin 2\theta \cos\varepsilon \sin\delta]$
I'_6	$I_b + \frac{I_a}{2}[1 + (1-\cos\delta)\sin 2\theta \cos 2\theta \sin\varepsilon - \cos 2\theta \cos\varepsilon \sin\delta]$
Replace ε by ε' for right circularly polarized light in the algorithm of Ajovalasit *et al.*	
Patterson and Wang	
I'_1	$I_b + \frac{I_a}{2}\{1 - (1-\cos\delta)\sin 2\theta \cos 2\theta + (\sin 2\theta - \cos 2\theta)\sin\delta \sin\varepsilon \cos\varepsilon + [\cos\delta + (1-\cos\delta)\sin 2\theta \cos 2\theta]\cos^2\varepsilon\}$
I'_2	$I_b + \frac{I_a}{2}\{1 + (1-\cos\delta)\sin 2\theta \cos 2\theta - (\sin 2\theta - \cos 2\theta)\sin\delta \sin\varepsilon \cos\varepsilon - [\cos\delta + (1-\cos\delta)\sin 2\theta \cos 2\theta]\cos^2\varepsilon\}$
I'_3	$I_b + \frac{I_a}{2}[1 + (\cos^2 2\theta + \sin^2 2\theta \cos\delta)\sin\varepsilon - \sin 2\theta \sin\delta \cos\varepsilon]$
I'_4	$I_b + \frac{I_a}{2}[1 + (1-\cos\delta)\sin 2\theta \cos 2\theta \sin\varepsilon + \cos 2\theta \cos\varepsilon \sin\delta]$
I'_5	$I_b + \frac{I_a}{2}[1 - (\cos^2 2\theta + \sin^2 2\theta \cos\delta)\sin\varepsilon + \sin 2\theta \sin\delta \cos\varepsilon]$
I'_6	$I_b + \frac{I_a}{2}[1 - (1-\cos\delta)\sin 2\theta \cos 2\theta \sin\varepsilon - \cos 2\theta \cos\varepsilon \sin\delta]$
Kihara	
I'_1	$I_a[1 + (1-\cos\delta)\sin 2\theta \cos 2\theta \sin\varepsilon + \sin 2\theta \sin\delta \cos\varepsilon]$
I'_2	$I_a[1 - (1-\cos\delta)\sin 2\theta \cos 2\theta \sin\varepsilon - \sin 2\theta \sin\delta \cos\varepsilon]$
I'_3	$I_a\{1 + [(1-\cos\delta)\cos^2 2\theta - 1]\sin\varepsilon + \cos 2\theta \sin\delta \cos\varepsilon\}$
I'_4	$I_a\{1 - [(1-\cos\delta)\cos^2 2\theta - 1]\sin\varepsilon - \cos 2\theta \sin\delta \cos\varepsilon\}$
I'_5	$I_a\left(\cos^2\frac{\delta}{2} + \sin^2\frac{\delta}{2}\cos^2 2\theta\right)$
I'_6	$I_a\left(\sin^2\frac{\delta}{2}\sin^2 2\theta\right)$
I'_7	$I_a\left(\cos^2\frac{\delta}{2} + \sin^2\frac{\delta}{2}\sin^2 2\theta\right)$
I'_8	$I_a\left(\sin^2\frac{\delta}{2}\cos^2 2\theta\right)$

Though the error in the quarter-wave plate modifies the intensity, it is clear from equation (10) that the evaluation of θ_c is not affected by it as $\cos\varepsilon$ cancels out in both the numerator and the denominator. However, experimentally significant error is obtained [Fig. 3(b)]. If ε is considered as the error for left circularly polarized light and ε' for right circularly polarized light then [**33**]

$$\theta_c = \frac{1}{2}\tan^{-1} \times \left[\frac{\begin{array}{l}\sin 2\theta(\cos\varepsilon' + \cos\varepsilon)\sin\delta \\ \quad + (\cos^2 2\theta + \sin^2 2\theta\cos\delta)(\sin\varepsilon' - \sin\varepsilon)\end{array}}{\begin{array}{l}\cos 2\theta(\cos\varepsilon' + \cos\varepsilon)\sin\delta \\ \quad - (1-\cos\delta)\sin 2\theta\cos 2\theta(\sin\varepsilon' - \sin\varepsilon)\end{array}} \right] \tag{11}$$

From equation (11) it can clearly be seen that the error term is not cancelled when compared to equation (10). Thus in the case of the six-step method of Ajovalasit *et al.*, the effect of ε' cannot be neglected in the isoclinic evaluation.

Similarly, using Table 4, for the method of Patterson and Wang, the isoclinic parameter obtained is

$$\theta_c = \frac{1}{2}\tan^{-1}\left(\frac{I'_5 - I'_3}{I'_4 - I'_6}\right) = \frac{1}{2}\tan^{-1}\left[\frac{\begin{array}{l}\sin 2\theta\cos\varepsilon\sin\delta \\ \quad - (\cos^2 2\theta + \sin^2 2\theta\cos\delta)\sin\varepsilon\end{array}}{\begin{array}{l}\cos 2\theta\cos\varepsilon\sin\delta \\ \quad + (1-\cos\delta)\sin 2\theta\cos 2\theta\sin\varepsilon\end{array}} \right] \tag{12}$$

and for the method of Kihara, the isoclinic parameter obtained is

$$\theta_c = \frac{1}{2}\tan^{-1}\left(\frac{I'_1 - I'_2}{I'_3 - I'_4}\right) = \frac{1}{2}\tan^{-1}\left\{ \frac{\begin{array}{l}\sin 2\theta\sin\delta\cos\varepsilon \\ \quad + (1-\cos\delta)\sin 2\theta\cos 2\theta\sin\varepsilon\end{array}}{\begin{array}{l}\cos 2\theta\sin\delta\cos\varepsilon \\ \quad + [(1-\cos\delta)\cos^2 2\theta - 1]\sin\varepsilon\end{array}} \right\} \tag{13}$$

Equations (12) and (13) clearly indicate the presence of the quarter-wave plate error in the isoclinic parameter obtained by the methodologies of Patterson and Wang and Kihara.

6 CONCLUSIONS

In this paper a comparative study on the evaluation of primary isoclinic data by various spatial domain methods based on circular, plane, and mixed polariscopes have been carried out both qualitatively and quantitatively. The study showed that the algorithms of Petrucci, Brown and Sullivan, and Mangal and Ramesh yield good results. For the isoclinic data along the line $y/R = 0.5$, the average absolute error is 1.98° using Petrucci's algorithm whereas it is 2.82° using Brown and Sullivan's algorithm and 3.75° for the algorithm of Mangal and Ramesh. For the isoclinic data along the line $y/R = 0.25$, the average absolute error is 1.66° using Petrucci's algorithm whereas it is 1.70° using Brown and Sullivan's algorithm and 4.95° for the algorithm of Mangal and Ramesh. Thus in summary, Petrucci's algorithm performs a little better than both Brown and Sullivan's algorithm and that of Mangal and Ramesh. The error is similar to that obtainable in a manual recording of isoclinics by conventional photoelasticity. The difference is that isoclinic data is obtained all over the domain. The error band in evaluating isoclinics is still quite high for stress separation studies. Hence, steps to smooth raw data are crucial for improving the accuracy of an evaluation of θ.

The methodologies involving quarter-wave plates give poor isoclinic values when compared to those using only a plane polariscope. Thus usage of methodologies involving only a plane polariscope is recommended for an isoclinic evaluation. There is a need to develop unwrapping schemes for obtaining θ in the range $-\pi/2$ to $+\pi/2$.

In all the methods, the expression for obtaining the isoclinics based on intensity processing is mathematically correct. However, results from the various methods using experimentally recorded images are not always the same. The causes of error can be traced to either improper handling of background intensity or mismatch of quarter-wave plates. Thus every effort must be made to account for the background intensity properly when proposing any new technique. It is also desirable that the role of quarter-wave plates on parameter estimation is assessed numerically.

The six-step phase-shifting method [**4**] has stood the test of time in accurately determining the value of the isochromatic parameter over the domain. However, the present study has showed that it is quite poor in estimating the value of the isoclinics. Thus if both the isochromatics and isoclinics need to be evaluated with reasonable accuracy two different

techniques may have to be used to estimate these. It is interesting to note that effort is already underway to combine the six-step method judicially with that of the plane polariscope methods in order to evaluate both the isochromatics and isoclinics with satisfactory accuracy [**34**].

All the digital polariscopes that are commercially available now use a quarter-wave plate for data acquisition and none of them use polarization stepping for isoclinic evaluation. More descriptions of commercially available digital polariscopes can be found in reference [**35**]. The designers of polariscopes need to account for the negative role of the quarter-wave plate for isoclinic evaluation by appropriate post-processing methods, or it would be better if the quarter-wave plates are avoided altogether. Use of the algorithm mentioned in reference [**34**] may be explored when designing a new polariscope to give both the isochromatic and isoclinic values with sufficient accuracy.

REFERENCES

1 **Ramesh, K.** *Digital photoelasticity: advanced techniques and application*, 2000 (Springer-Verlag, Berlin, Germany).
2 **Patterson, E. A.** and **Wang, Z. F.** Towards full field automated photoelastic analysis of complex components. *Strain*, 1991, **27**(2), 49–56.
3 **Asundi, A.** Phase shifting in photoelasticity. *Expl Techniques*, 1993, **17**(1), 19–23.
4 **Ajovalasit, A., Barone, S.,** and **Petrucci, G.** A method for reducing the influence of the quarter-wave plate error in phase-shifting photoelasticity. *J. Strain Analysis*, 1998, **33**(3), 207–216.
5 **Kihara, T.** Automatic whole-filed measurement of photoelasticity using linear polarized incident light. In Proceedings of the 9th International Conference of *Experimental mechanics*, Copenhagen, Denmark, 1990, Vol. 2, pp. 821–827.
6 **Dupré, J. C., Brémand, F.,** and **Lagarde, A.** Photoelastic data processing through digital image processing: isostatics and isochromatics reconstruction. Presented at the International Conference on *Photoelasticity: new instrumentation, materials and data processing techniques*, London, 1993 (SIRA Communications, Chislehurst).
7 **Sarma, V. S. S. S. R., Pillai, S. A., Subramanian, G.,** and **Varadan, T. K.** Computerized image processing for whole-filed determination of isoclinics and isochromatics. *Expl Mechanics*, 1992, **32**(1), 24–29.
8 **Mangal, S. K.** *Data acquisition in digital photoelasticity by phase shifting techniques*, PhD Thesis, Department of Mechanical Engineering, Indian Institute of Technology, Kanpur, India, 1999.
9 **Mangal, S. K.** and **Ramesh, K.** Use of multiple loads to extract continuous isoclinic fringes by phase-shifting. *Strain*, 1999, **35**(1), 15–17; Errata 1999, **35**(2), 76.
10 **Kihara, T.** Automatic whole-field measurement of principal stress directions using three wavelengths. In Proceedings of the 10th International Conference on *Experimental mechanics*, Lisbon, 1994, Vol. 1, pp. 95–99.
11 **Nurse, A. D.** Full-field automated photoelasticity using a three-wavelength approach to phase-shifting. *Appl. Optics*, 1997, **36**, 5781–5786.
12 **Lei Zhenkun, Yun Dazhen,** and **Yu Wamming.** Whole-field determination of isoclinic parameter by five-step color phase shifting and its error analysis. *Optics and Lasers in Engng*, 2003, **40**, 189–200.
13 **Morimoto, Y., Morimoto Jr, Y.** and **Hayashi, T.** Seperation of isochromatics and isoclinics using Fourier transform. *Expl Techniques*, 1994, **18**(5), 13–17.
14 **Lesniak, J. R.** and **Zickel, M. J.** Applications of automated grey-field polariscope. In Proceedings of the SEM Spring Conference on *Experimental and Applied Mechanics*, Houston, Texas, 1998, pp. 298–301.
15 **Brown, G. M.** and **Sullivan, J. L.** The computer-aided holophotoelastic method. *Expl Mechanics*, 1990, **30**(2), 135–144.
16 **Mawatari, S., Takashi, M., Toyada, Y.,** and **Kunio, T.** A single valued representative function for determination of principal stress direction in photoelastic analysis. In Proceedings of the 9th International Conference on *Experimental mechanics*, Copenhagen, 1990, Vol. 5, pp. 2069–2078.
17 **Buckberry, C.** and **Towers, D.** New approaches to the full-field analysis of photoelastic stress patterns. *Optics and Lasers in Engng*, 1996, **24**, 415–428.
18 **Chen, T. Y.** and **Lin, C. H.** An improved method for whole field automatic measurement of principal stress direction. In abstract of the Proceedings of the 8th International Conference on *Experimental mechanics*, Nashville, USA, 1996, 178–179.
19 **Petrucci, G.** Full-field automatic evaluation of an isoclinic parameter in white light. *Expl Mechanics*, 1997, **37**(4), 420–426.
20 **Ng, T. W.** Photoelastic stress analysis using an object step loading method. *Expl Mechanics*, 1997, **37**(2), 137–141.
21 **Ekman, M. J.** and **Nurse, A. D.** Completely automated determination of two dimensional photoelastic parameters using load stepping. *Optical Engng*, 1998, **37**(6), 1845–1851.
22 **Ramesh, K.** and **Tamrakar, D. K.** Improved determination of retardation in digital photoelasticity by load stepping. *Optics and Lasers in Engng*, 2000, **33**, 387–400.

23 **Wang, Z. F.** and **Patterson, E. A.** Use of phase-stepping with demodulation and fuzzy sets for birefringence measurement. *Optics and Lasers in Engng*, 1995, **22**, 91–104.

24 **Siegmann, P., Backman, D.,** and **Patterson, E. A.** A robust approach to demodulating and unwrapping phase-stepped photoelastic data. *Expl Mechanics*, 2005, **45**(3), 278–289.

25 **Andrei, E., Anton, J.,** and **Aben, H.** On data-processing in photoelastic residual stress measurement in glass. In Proceedings of the International Conference on *Experimental mechanics* (*ICEM 05*), New Delhi, 10–15 September 2005.

26 **Patterson, E. A.** and **Wang, Z. F.** Simultaneous observation of phase stepped images for automated photoelasticity. *J. Strain Analysis*, 1998, **33**(1), 1–15.

27 **Asundi, A., Sajan, M. R.,** and **Liu Tong** Dynamic photoelasticity by TDI imaging. *Optics and Lasers in Engng*, 2002, **38**, 3–16.

28 **Lesniak, J. R., Zhang, S. J.,** and **Patterson, E. A.** Design and evaluation of the poleidoscope: a novel digital polariscope. *Expl Mechanics*, 2004, **44**, 128–135.

29 **Ramesh, K.** PHOTOSOFT_H: a comprehensive photoelasticity simulation module for teaching the technique of photoelasticity. *Int. J. Mech. Engng Education*, 1997, **25**(4), 306–324.

30 **Timoshenko, S.** On the distribution of stresses in a circular ring compressed by two forces acting along a diameter. *Phil. Mag.*, 1992, S-6, **44**(263), 1014–1019.

31 **Sai Prasad, V.** and **Ramesh, K.** Background intensity effects on various phase shifting techniques in photoelasticity. In Proceedings of the Conference on *Optics and photonics in engineering*, New Delhi, 2003.

32 **Tamrakar, D. K.** and **Ramesh, K.** Simulation of errors in digital photoelasticity by Jones calculus. *Strain*, 2001, **37**(3), 105–112.

33 **Ajovalasit, A., Barone, S., Petrucci, G.,** and **Zuccarello, B.** The influence of the quarter wave plates in automated photoelasticity. *Optics and Lasers in Engng*, 2002, **38**, 31–56.

34 **Barone, S., Burriesci, G.,** and **Petrucci, G.** Computer aided photoelasticity by an optimum phase stepping method. *Expl Mechanics*, 2002, **42**(2), 132–139.

35 **Ramesh, K.** Photoelasticity. In *Springer handbook on experimental solid mechanics* (Ed. W. N. Sharpe), July 2006 (Springer-Verlag, Berlin).

APPENDIX

Notation

I_a	light intensity accounting for the amplitude of light
I_b	background or stray light intensity
I_i	intensity of light transmitted for the ith optical arrangement corresponding to the loaded image
I_i'	intensity of light transmitted for the ith optical arrangement corresponding to the loaded image incorporating the quarter-wave plate error
I_i''	intensity of light transmitted for the ith optical arrangement corresponding to the reconstructed dark-field loaded image
$I_{i,j}$	intensity of light transmitted for the ith optical arrangement corresponding to the loaded image respectively for red, green, and blue planes (j = R, G, B)
I_{ui}	intensity of light transmitted for the ith optical arrangement corresponding to the unloaded image
α	orientation of the polarizer axis from the x axis
β	orientation of the analyser axis from the x axis
δ	retardation introduced by the model
ε	quarter-wave plate error (rad)
ε'	quarter-wave plate error (rad) due to a non-homogeneous quarter-wave plate
η	orientation of the slow axis of the second quarter-wave plate from the x axis
θ	orientation of the principal stress direction (rad) from the x axis
θ_c	calculated value of the principal stress direction (rad)
λ	wavelength of the light source (nm)
λ_{ref}	reference wavelength for the quarter-wave plates (nm)
ξ	orientation of the slow axis of the first quarter-wave plate from the x axis
σ_1, σ_2	principal stresses ($\sigma_1 > \sigma_2$)